A Novel Harmonic Current Control Method for Torque Ripple Reduction of SPMSM Considering DC-Link Voltage Limit

Zekai Lyu, *Graduate Student Member, IEEE*, Lijian Wu, *Senior Member, IEEE*, and Pingyue Song

***Abstract*—Torque ripple reduction based on harmonic current injection has been widely applied to surface-mounted permanent-magnet synchronous machine (SPMSM) drive systems. However, additional voltages are typically required for harmonic injection, and the dc-link voltage limit should be considered in practical drive systems. This article proposes a novel harmonic control for SPMSMs in which the torque ripple reduction and high dc-link voltage utilization can be achieved simultaneously. The influence of harmonic injection on voltage utilization is investigated in detail. In addition to injecting the appropriate *q*-axis harmonic currents to suppress torque ripple, the *d*-axis harmonics are also optimized and injected. The geometric principle is applied to obtain the analytical expression for the optimal *d*-axis harmonic voltage, which can minimize the maximum magnitude of the stator voltage vector. Since the reference harmonic voltage is directly calculated in accordance with the analytical solution, the implementation complexity of harmonic voltage regulation is relatively low. Moreover, a virtual dual three-phase system with auxiliary currents is developed to decompose the fundamental and harmonic currents without low-pass filters, thus avoiding additional delay in the control loop. Finally, the experimental results are provided to verify the validity of the proposed method.**

***Index Terms*—Geometric principle, harmonic current injection, surface-mounted permanent-magnet synchronous machine (SPMSM), torque ripple reduction, voltage utilization.**

I. Introduction

PERMANENT-MAGNET (PM) machines have been widely used in electric vehicles, wind power generation, and other industrial applications for their high efficiency and high power density [1], [2], [3], [4], [5], of which the surface-mounted PM synchronous machine (SPMSM) is an important type with simple construction and excellent performance. The torque ripple is one of the significant issues of machine drive system, which can induce undesirable mechanical vibration and acoustic noise [6], [7], [8]. Hence, torque ripple reduction has drawn increased attention in both academic and industrial research.

Typically, techniques for reducing torque ripple can be divided into two categories: methods based on machine design and methods based on machine control [9]. The first one mainly involves the optimization of design parameters. In [10], [11], [12], and [13], several approaches, such as magnet shifting, rotor/stator skewing, and magnet shaping, were investigated to lessen the torque ripple by reducing the cogging torque and harmonics in PM flux linkage. However, these strategies may also reduce the average torque or increase manufacturing complexity. In practical PM machines, it is inevitable that harmonics exist in the PM flux linkage and back-electromotive force (EMF) due to design tradeoffs and manufacturing tolerances [14]. Hence, torque ripple reduction from the machine control perspective is usually required, which is also the focus of this article.

Due to the limited ac signal tracking capability, the commonly used proportional–integral (PI) regulator cannot well eliminate current distortions in the *d*–*q* frame. To reduce the torque ripple, several works about harmonic current suppression have been carried out with the target of sinusoidal current excitation. In [15] and [16], the $(6n\pm1)$th harmonics in the stator currents caused by inverter nonlinearity were analyzed and compensated. The current distortions caused by error between the reference voltage and the actual output voltage can be effectively suppressed. Additionally, harmonic suppression based on PM flux-linkage harmonics identification and PI–resonant regulator was proposed in [17] to deal with the disturbance caused by machine side, that is, nonsinusoidal back EMFs. In [18], the fundamental and harmonic currents were separated by multiple synchronous rotating frame (MSRF) transformations and controlled by conventional PI regulators, respectively. The methods mentioned above are valid and contribute to attenuating the harmonic currents. However, as mentioned above, harmonics will unavoidably be present in the back-EMFs of practical machines. Hence, in some cases, sinusoidal current excitation cannot ensure the minimum torque ripple, and optimal harmonic current injection is meaningful.

To suppress the intrinsic torque ripple, the injected harmonic currents can be designed properly to produce additional harmonic torque with the same magnitude but opposite in phase of the existing harmonic torque. The approaches for determining the amplitude and phase of reference harmonic currents can be classified into two categories: methods based on the

Manuscript received 4 July 2023; revised 22 September 2023; accepted 30 October 2023. Date of publication 3 November 2023; date of current version 22 December 2023. This work was supported by the National Natural Science Foundation of China under Grants 52225703 and 51977191. Recommended for publication by Associate Editor N. Idris. *(Corresponding author: Lijian Wu.)*

The authors are with the College of Electrical Engineering, Zhejiang University, Hangzhou 310027, China (e-mail: zklyu@zju.edu.cn; ljw@zju.edu.cn; py_song@zju.edu.cn).

Color versions of one or more figures in this article are available at https://doi.org/10.1109/TPEL.2023.3329934.

Digital Object Identifier 10.1109/TPEL.2023.3329934

torque model [19], [20], [21] and methods based on speed feedback [22], [23], [24]. In [19], the q-axis harmonic current reference was generated by a lookup table of back EMF and regulated by the repetitive controller. Furthermore, to counteract the fundamental and second-order harmonic components of the cogging torque for a flux-switching PM machine, a series of harmonics were injected in the q-axis reference current [20]. In addition to compensating for the influence of PM flux-linkage harmonics and cogging torque, the reference harmonic current calculation can also take the stator copper losses into account [21]. Also, there are several methods using the speed feedback to obtain the reference value of harmonic currents, which can omit the offline measurements of machine parameters. In [22], PI–resonant regulators were employed in both speed control loop and current control loop to reject periodic torque ripples. Moreover, the magnitude and phase of the speed harmonic were extracted in [23], which makes it possible to determine the reference harmonic using the conventional PI controller. Also, the optimization algorithms, such as gradient descent optimization, can also be used to obtain the reference harmonic currents [24].

It should be noted that, whether through harmonic current suppression or optimized harmonic current injection, a certain harmonic voltage must be generated to regulate harmonic current, which can increase the magnitude of the output voltage vector. Nevertheless, in practice, the maximum possible voltage vector is limited by the dc-link voltage. To produce the optimal harmonic voltage, the amplitude of the maximum achievable fundamental voltage will be decreased, which will result in the reduction of the maximum operation speed and maximum output torque of machine. However, in the previous literature, reducing torque ripple with the consideration of dc-link voltage utilization is rarely investigated except [25] and requires further research. In [25], several low-pass filters (LPFs) and one bandpass filter (BPF) were used to extract harmonic components in stator current and voltage, which can bring a significant delay in the control loop.

The harmonic detection also plays an important role in torque ripple reduction. Limited by only two degrees of control freedoms for the three-phase machine with a common neutral point, the fundamental and harmonic currents are coupled together and difficult to separate. Hence, LPFs are usually needed in MSRF-based harmonic control [18], [23], [24]. Note that the delay resulting from LPFs can degrade the dynamic performance as well as the stability margin of the control system. It is worth mentioning that the dual three-phase machine has more degrees of control freedom and more decoupled dimensions. By using vector space decomposition (VSD) [26], per-phase variables, such as the current, the voltage, and the flux, can be directly mapped into different orthogonal subspaces, allowing the separation of harmonics with different orders. On this basis, a novel decomposition transformation combined with auxiliary currents was proposed for dual three-phase PMSM [27], which can further increase decoupled dimensions. However, current harmonics detection in the standard three-phase PMSM without using digital filters has not been well discussed so far; especially when considering voltage limit, the detection of harmonic voltages also requires the adoption of such filters.

In light of the above discussions, this article proposes a novel harmonic current control scheme for torque ripple reduction of SPMSM, by which the high dc-link voltage utilization can be realized. In addition to injecting appropriate q-axis harmonic current to suppress torque ripple, the d-axis harmonic is also optimized to minimize the maximum magnitude of the stator voltage vector. The analysis of the voltage utilization considering harmonic injection is derived in detail. A geometric principle-based method is proposed to demonstrate the analytical solution for the reference d-axis harmonic voltage. Moreover, harmonic decomposition based on a virtual dual three-phase system is proposed to decompose the fundamental and harmonic currents. The proposed scheme does not involve complex optimization strategies and any digital filters, so it is computationally efficient and can work well under both steady-state and dynamic conditions. Finally, comparative experimental results are presented to verify the improved performance compared with the conventional methods.

II. Modeling and Harmonic Analysis of SPMSM

Assuming that the machine windings are balanced, the voltage equation of the PM machine can be expressed as

$$\begin{bmatrix} u_a \\ u_b \\ u_c \end{bmatrix} = R_s \begin{bmatrix} i_a \\ i_b \\ i_c \end{bmatrix} + \begin{bmatrix} L & M & M \\ M & L & M \\ M & M & L \end{bmatrix} p \begin{bmatrix} i_a \\ i_b \\ i_c \end{bmatrix} + \begin{bmatrix} e_a \\ e_b \\ e_c \end{bmatrix} \quad (1)$$

where p is the derivative operator, R_s is the stator resistance, L and M are the self and mutual winding inductances, and $u_{a,b,c}$, $i_{a,b,c}$, and $e_{a,b,c}$ are the three-phase stator voltages, phase currents, and back-EMFs, respectively. The conventional field-oriented control (FOC) is conducted in a synchronous rotating frame (d–q frame), where (1) can be rewritten as

$$\begin{bmatrix} u_d \\ u_q \end{bmatrix} = R_s \begin{bmatrix} i_d \\ i_q \end{bmatrix} + \begin{bmatrix} pL_d & -\omega_e L_q \\ \omega_e L_d & pL_q \end{bmatrix} \begin{bmatrix} i_d \\ i_q \end{bmatrix} + \omega_e \begin{bmatrix} -\psi_{fq} \\ \psi_{fd} \end{bmatrix} \quad (2)$$

where ω_e is the angular velocity of rotor, u_d, u_q and i_d, i_q are the stator voltages and currents in the d–q frame, L_d and L_q are the d- and q-axis inductances, and R_s is the stator resistance. Additionally, ψ_{fd} and ψ_{fq} represent the PM flux linkages in d–q frame, while $\omega_e\psi_{fq}$ and $\omega_e\psi_{fd}$ denote the back EMFs in d–q frame. The electromagnetic torque can be expressed as

$$T_e = 1.5n_p \left[\left(\psi_{fd} + L_d i_d \right) i_q - \left(\psi_{fq} + L_q i_q \right) i_d \right] \quad (3)$$

where n_p is the number of pole pairs. Ideally, as long as i_d and i_q are dc components, the torque ripple can be well suppressed. However, as aforementioned, the back EMFs in practical PM machines are usually not ideal sinusoidal, which can affect the output torque. The measured phase back EMF waveforms of a 12-slot/10-pole prototype machine at 500 r/min are presented in Fig. 1(a), and the harmonic spectrum of phase-a back EMF is shown in Fig. 1(b). The back EMF mainly includes the third-, fifth-, and seventh-order harmonics with amplitudes of 5.2%, 5.4%, and 1.5% of the fundamental component, respectively. The triplen harmonics are zero-sequence components, which do not exist in line back EMFs of a balanced Y-connected three-phase circuit. Therefore, the fifth- and seventh-order harmonics

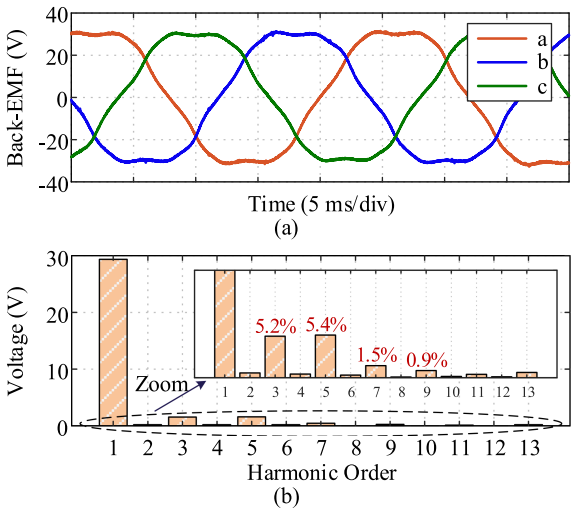

Fig. 1. Measured back EMF waveforms and spectrum. (a) Three-phase back EMFs. (b) Harmonic spectrum.

are dominant harmonics that can affect the operation of the investigated PMSM. The three-phase back-EMFs considering the main harmonics can be expressed as

$$\begin{cases} e_a = -\omega_e\psi_1\sin(\omega_e t) - 5\omega_e\psi_5\sin(5\omega_e t+\theta_5) \\ \qquad -7\omega_e\psi_7\sin(7\omega_e t+\theta_7) \\ e_b = -\omega_e\psi_1\sin(\omega_e t-2\pi/3) - 5\omega_e\psi_5\sin(5\omega_e t+2\pi/3+\theta_5) \\ \qquad -7\omega_e\psi_7\sin(7\omega_e t-2\pi/3_1+\theta_7) \\ e_c = -\omega_e\psi_1\sin(\omega_e t+2\pi/3) - 5\omega_e\psi_5\sin(5\omega_e t-2\pi/3+\theta_5) \\ \qquad -7\omega_e\psi_7\sin(7\omega_e t+2\pi/3+\theta_7) \end{cases} \tag{4}$$

where ψ_1, ψ_5, and ψ_7 are the harmonic amplitudes of the fundamental, fifth- and seventh-order PM flux linkages, respectively, and θ_5 and θ_7 are the initial phase angles of two harmonic components. In *a–b–c* frame, the fifth-order harmonic is with negative sequence and the seventh-order harmonic is with positive sequence. Then, the PM flux linkages in the *d–q* frame can be rewritten as

$$\begin{bmatrix}\psi_{fd}\\ \psi_{fq}\end{bmatrix} = \begin{bmatrix}\psi_1 - \psi_5\cos(6\omega_e t+\theta_5) + \psi_7\cos(6\omega_e t+\theta_7)\\ \psi_5\sin(6\omega_e t+\theta_5) + \psi_7\sin(6\omega_e t+\theta_7)\end{bmatrix}. \tag{5}$$

As can be seen, the PM flux linkages in *d–q* frame contain the sixth-order harmonics, which can cause current distortion and torque ripple. Note that the number of pole pairs for fifth-order harmonics equals $5n_p$ and the number of pole pairs for seventh-order harmonics equals $7n_p$. For SPMSM, where the inductance on the *d*-axis is approximately equal to the inductance on the *q*-axis, $i_d = 0$ current control is usually applied. Then, considering the harmonics of stator currents and PM flux linkages, (3) can be rewritten as

$$\begin{aligned} T_e &= 1.5n_p \\ &\times \begin{bmatrix} \psi_1 i_{qf} + \psi_1 i_{qh} \\ +\left(-5\psi_5\cos(6\omega_e t+\theta_5) + 7\psi_7\cos(6\omega_e t+\theta_7)\right) i_{qf} \\ +\left(-5\psi_5\cos(6\omega_e t+\theta_5) + 7\psi_7\cos(6\omega_e t+\theta_7)\right) i_{qh} \end{bmatrix} \end{aligned} \tag{6}$$

where i_{qf} and i_{qh} represent the fundamental current and harmonic current of the *q*-axis, respectively. Note that only harmonic components in stator currents and PM flux are considered because the magnitudes of inductance harmonics are relatively small. The torque in (6) can be seen as a combination of four items: the interaction between fundamental current and fundamental flux linkage, the interaction between harmonic current and fundamental flux linkage, the interaction between fundamental current and harmonic flux linkage, and the interaction between harmonic current and harmonic flux linkage. The first item represents the main average torque and the second and third terms represent the torque ripple. The product of the harmonic current and harmonic flux linkage can be neglected because of its low amplitude and high frequency [21]. To attenuate the sixth-order torque, harmonic current can be injected to make the sum of the second and third items equal to 0. Hence, the reference of injected harmonic current should satisfy

$$i_{qh}^{*} = \frac{i_{qf}}{\psi_1}\left[5\psi_5\cos(6\omega_e t+\theta_5) - 7\psi_7\cos(6\omega_e t+\theta_7)\right]. \tag{7}$$

III. Analysis of DC-Link Voltage Utilization

A. Voltage Utilization Considering Harmonics

Whether for current harmonic suppression or current harmonic injection, the optimal harmonic voltages should be added to the output voltage. Considering the fifth- and seventh-order harmonics of *a–b–c* frame, the *dq*-axes reference voltages can be expressed as

$$\begin{cases} u_d = u_{df} + u_{dh} = u_{df} + U_5\cos(-6\omega_e t+\varphi_5) \\ \qquad +U_7\cos(6\omega_e t+\varphi_7) \\ u_q = u_{qf} + u_{qh} = u_{qf} + U_5\sin(-6\omega_e t+\varphi_5) \\ \qquad +U_7\sin(6\omega_e t+\varphi_7) \end{cases} \tag{8}$$

where u_{df} and u_{qf} represent the fundamental components of the *dq* axes stator voltages, U_5 and U_7 are the amplitudes of the fifth- and seventh-harmonic voltages, and φ_5 and φ_7 are the initial phase angles of the fifth- and seventh-harmonic voltages. With the harmonic voltage injection, the total voltage vector is the combination of the fundamental voltage vector and the harmonic voltage vectors, which can be expressed as

$$\vec{u}_s = \vec{u}_f + \vec{u}_5 + \vec{u}_7 \tag{9}$$

where $\vec{u}_f$ represents the fundamental voltage vector, and $\vec{u}_5$ and $\vec{u}_7$ represent the fifth- and seventh-order harmonic voltage vector, respectively.

Fig. 2 shows the voltage vector trajectory with harmonic injection. According to the linear modulation range for space vector pulsewidth modulation (SVPWM), the maximum amplitude of the voltage vector is $u_{\mathrm{dc}}/\sqrt{3}$. The system voltage constraint equation is given as

$$|\vec{u}_s| = \sqrt{u_d^2 + u_q^2} \le \frac{u_{\mathrm{dc}}}{\sqrt{3}} \tag{10}$$

where u_{dc} is the dc-link voltage. Obviously, when the harmonic voltages are injected, the amplitude of the voltage vector will increase and may even exceed the voltage limit. Note that the trajectory out of the boundary is not feasible due to the voltage

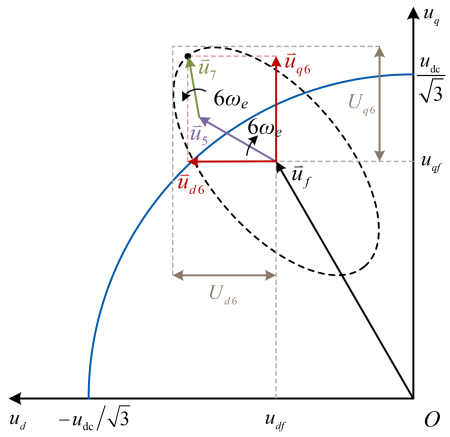

Fig. 2. Voltage vector trajectory with harmonic injection.

limit of the inverter. As for the inverter operating with SVPWM, the dc-link voltage utilization, i.e., the ratio of the maximum amplitude of the fundamental line–line voltage to the dc voltage, is equal to 1 when there is no harmonic injection. However, when the harmonic voltages are injected, the proportion of fundamental voltage will become smaller when the total voltage trajectory reaches the boundary. The voltage utilization considering harmonic injection can be expressed as

$$m = \frac{|\vec{u}_f|}{|\vec{u}_s|} = \frac{|\vec{u}_f|}{|\vec{u}_f + \vec{u}_5 + \vec{u}_7|}. \tag{11}$$

In other words, the harmonic injection can lead to the decrease of the dc-link voltage utilization and maximum output fundamental voltage. The amplitude of the fundamental voltage will affect the maximum operation speed and maximum output torque of the PMSM. Hence, the harmonic injection may degrade the system performance when the voltage limit is considered.

It is noteworthy that both the fifth- and seventh-order harmonics under the *a–b–c* frame are transformed to the harmonics with six times the electrical frequency in the *d–q* frame. By synthesizing the projection of the reference vectors on the *d*-axis and the *q*-axis, the harmonic voltage vectors can be regarded as the combination of two orthogonal vectors $\vec{u}_{d6}$ and $\vec{u}_{q6}$. These two vectors are, respectively, along the direction of the *d*-axis and the *q*-axis. The amplitude of two vectors can be expressed as

$$\begin{cases} |\vec{u}_{d6}| = U_{d6}\cos(6\omega_e t + \varphi_{d6}) \\ |\vec{u}_{q6}| = U_{q6}\cos(6\omega_e t + \varphi_{q6}) \end{cases} \tag{12}$$

where U_{d6} and U_{q6} represent the amplitudes and φ_{d6} and φ_{q6} represent the initial phase angles. As shown in Fig. 2, the amplitude of the total voltage vector can be regulated by adjusting $\vec{u}_{d6}$ and $\vec{u}_{q6}$, which will be discussed in Section III-B.

B. Optimal D*-Axis Harmonic Injection for Improving DC-Link Voltage Utilization*

According to (7), injecting optimal *q*-axis harmonic current can suppress the torque ripple. Hence, the optimal *q*-axis harmonic voltage can be determined according to the objective of better torque performance. It is worth noting that, as for SPMSMs, the *d*-axis harmonic current typically does not generate a large torque ripple. Therefore, the *d*-axis harmonic voltage can be regulated to reduce the maximum amplitude of the stator voltage vector as much as possible, thus improving the dc-link voltage utilization.

Fig. 3 shows the voltage vector trajectories with different U_{d6} and φ_{d6}. It should be noted that a smaller maximum distance from the voltage trajectory to the origin is expected. The relation between the voltage vector trajectory and φ_{d6} is shown in Fig. 3(a). Generally, the trajectory is an ellipse in which the fundamental voltage vector determines the center of the ellipse, and the harmonic voltage vector determines the size and shape of the ellipse. The shape of the voltage trajectory changes with the increase of φ_{d6}, but it will always be inscribed with the rectangle determined by U_{d6} and U_{q6}. According to the geometric relationship, it can be concluded that in the current situation (i.e., the second quadrant), only if $\varphi_{d6} = \varphi_{q6}$, as shown by the cyan line in Fig. 3(a), the maximum distance from the voltage trajectory to the origin can be the smallest.

The design objective for the *d*-axis harmonic injection is to improve the voltage utilization, that is, to minimize the maximum magnitude of the voltage vector, which can be expressed as

$$\min_{U_{d6},\varphi_{d6}} r_{\max} \text{ s.t. } |\vec{u}_f + \vec{u}_{d6} + \vec{u}_{q6}| \le \frac{u_{dc}}{\sqrt{3}}, \varphi_{d6} = \varphi_{q6}. \tag{13}$$

The relation between the voltage vector trajectory and U_{d6} is shown in Fig. 3(b) and (c). Noted that $\varphi_{d6} = \varphi_{q6}$ is satisfied so that the trajectory is a line segment. It can be seen that, with the change of U_{d6}, the midpoint of the line segment remains unchanged, while the two endpoints move in the opposite direction. Hence, the maximum amplitude of the voltage vector depends on the maximum distance between the two endpoints of the line segment and the origin, which can be denoted as

$$|\vec{u}_s|_{\max} = r_{\max} = \max\{r_1, r_2\} \tag{14}$$

where r_1 and r_2 represent the distances between the endpoints and the origin, and $r_{\max}$ represents the maximum of the two. In Fig. 3(b), according to the presented geometric relationship, only when the harmonic voltage trajectory is perpendicular to the fundamental voltage vector (as shown by the purple dashed line), $r_{\max}$ is minimum and can be expressed as

$$\min_{U_{d6},\varphi_{d6}} r_{\max} = r_1 = r_2 = \sqrt{u_{qf}^2 + u_{df}^2 + U_{q6}^2 + U_{d6}^2} \tag{15}$$

where U_{d6} is the optimal amplitude of harmonic voltage. According to the property of the similar triangles, the optimized U_{d6} can be expressed as

$$U_{d6} = -\frac{u_{qf}U_{q6}}{u_{df}}, \left(u_{df} < 0 \text{ and } u_{df} < \frac{u_{qf}U_{q6}}{u_{df}}\right). \tag{16}$$

It is noted that, as for the case shown in Fig. 3(c), when the harmonic voltage trajectory passes through point $(0, u_{qf}+U_{q6})$ (as shown by the purple dashed line), $r_{\max}$ is the minimum and can be expressed as

$$\min_{U_{d6},\varphi_{d6}} r_{\max} = r_1 = u_{qf} + U_{q6}. \tag{17}$$

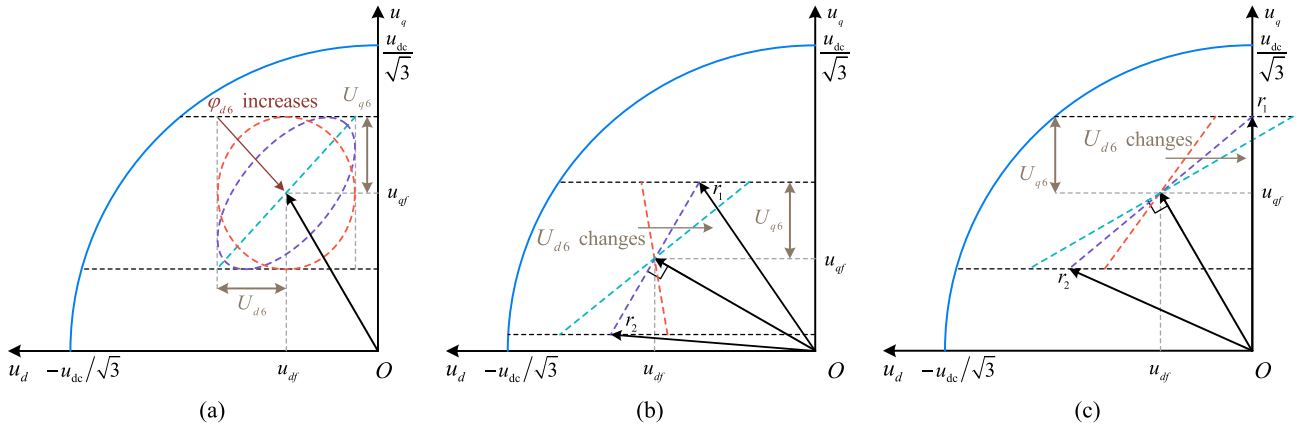

Fig. 3. Voltage vector trajectories with different U_{d6} and φ_{d6}. (a) Case I. (b) Case II. (c) Case III.

In this case, the optimal amplitude of harmonic voltage U_{d6} is equal to the amplitude of u_{df}, which can be expressed as

$$U_{d6} = -u_{df}, \left(u_{df} < 0 \text{ and } u_{df} \geq \frac{u_{qf}U_{q6}}{u_{df}}\right). \tag{18}$$

The above analysis is carried out for conditions with $u_{df} < 0$. Meanwhile, for the conditions with $u_{df} = 0$ and $u_{df} > 0$, the proposed method based on geometric principle can also be used to optimize the d-axis harmonic voltage. The amplitude and phase angle of d-axis harmonic voltage, which can minimize the maximum stator voltage amplitude, are, respectively, expressed as follows:

$$\begin{cases} U_{d6} = \min\left\{|u_{df}|, \left|\frac{u_{qf}U_{q6}}{u_{df}}\right|\right\}, (u_{df} \neq 0) \\ U_{d6} = 0, (u_{df} = 0) \end{cases} \tag{19}$$

$$\begin{cases} \varphi_{d6} = \varphi_{q6}, (u_{df} \leq 0) \\ \varphi_{d6} = \varphi_{q6} + \pi, (u_{df} > 0). \end{cases} \tag{20}$$

It should be noted that although the presented analysis is about sixth-order torque ripple and voltage fluctuation, it is also applicable to harmonic regulation with other frequencies. For instance, the 12th-order torque ripple might be dominant for PMSM with other slot/pole combinations. Similar to the 6th-order torque ripple reduction, the 11th- and 13th-order harmonic currents can be injected in phase currents to suppress the 12th-order torque ripple. There will correspondingly be 12th-order fluctuations in stator voltage amplitude. Then, using the presented geometric principle, the amplitudes U_{d12} and initial phase angle φ_{d12} of the d-axis harmonic voltage can be optimized to reduce the maximum amplitude of the stator voltage.

IV. Proposed Control Method

In this section, a novel active harmonic current injection scheme is proposed. There are two aims expected, namely, to suppress the torque ripple by injecting q-axis harmonic current and to reduce the voltage fluctuations by adjusting the d-axis harmonic voltage. The proposed scheme consists of three parts:

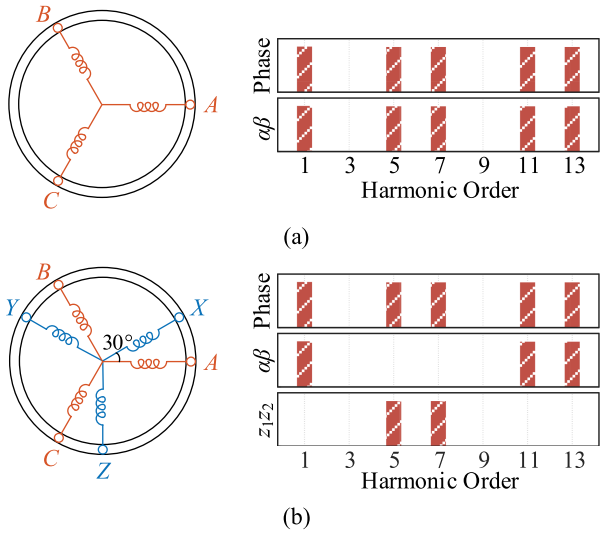

Fig. 4. Harmonic mapping of PMSMs. (a) Single three-phase machine. (b) Dual three-phase machines.

1) harmonic decomposition based on a virtual dual three-phase system;
2) q-axis harmonic current control and its amplitude calculation;
3) d-axis harmonic voltage regulation based on the presented geometric principle.

A. Harmonic Current Decomposition Based on Virtual Dual Three-Phase System

Fig. 4 presents the harmonic mapping of single three-phase machine and asymmetrical dual three-phase machines. As shown in Fig. 4(a), for standard three-phase PMSMs, all components are mapped to the $\alpha\beta$ space after applying the Clark transformation. Therefore, the current harmonics cannot be extracted directly. The conventional approaches of harmonic current detection are typically based on LPFs, which can cause a significant delay and affect the dynamic performance of the system.

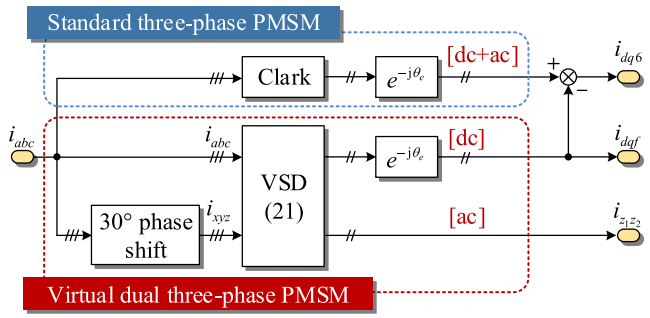

Fig. 5. Harmonic current detection based on virtual dual three-phase systems.

Significantly, the components of the multi-three-phase PMSM can be decoupled into several orthogonal subspaces by using the VSD method [26]. As for asymmetric dual three-phase machines, where two sets of windings (A, B, C) and (X, Y, Z) are spatially shifted 30 electrical degrees with two neutral points, the transformation can be expressed as

$$\begin{aligned}&\begin{bmatrix}F_\alpha & F_\beta & F_{z_1} & F_{z_2}\end{bmatrix}^T\\&= [T_{\mathrm{VSD}}]\begin{bmatrix}F_A & F_X & F_B & F_Y & F_C & F_Z\end{bmatrix}^T\end{aligned} \tag{21}$$

where variable F can denote voltage, current, or flux linkage, $[T_{\mathrm{VSD}}]$ represents the transformation matrix, subscripts α and β represent the subspace comprising the fundamental components, and subscripts z_1 and z_2 represent the subspace comprising the harmonic components. $[T_{\mathrm{VSD}}]$ can be expressed as follows:

$$[T_{\mathrm{VSD}}] = \frac{1}{3}\begin{bmatrix}1 & \cos(\alpha) & \cos(4\alpha) & \cos(5\alpha) & \cos(8\alpha) & \cos(9\alpha)\\0 & \sin(\alpha) & \sin(4\alpha) & \sin(5\alpha) & \sin(8\alpha) & \sin(9\alpha)\\1 & \cos(5\alpha) & \cos(8\alpha) & \cos(\alpha) & \cos(4\alpha) & \cos(9\alpha)\\0 & \sin(5\alpha) & \sin(8\alpha) & \sin(\alpha) & \sin(4\alpha) & \sin(9\alpha)\end{bmatrix} \tag{22}$$

where $\alpha = \pi/6$. The harmonic mapping of dual three-phase machines is presented in Fig. 4(b), in which the fundamental and harmonic components in the order of $12n\pm1$ ($n = 1, 2, 3, \ldots$) are mapped into the $\alpha\beta$ subspace, and the harmonic components in the order of $12n\pm5$ ($n = 0, 1, 2, \ldots$) are mapped into the z_1z_2 subspace. Note that the zero-sequence harmonics in the order of $3n$ ($n = 1, 3, 5, \ldots$) are not considered due to the isolated neutral point winding structure. As can be seen, the fifth- and seventh-order harmonic components are decomposed from the fundamental component.

In this article, the harmonic current detection based on the virtual dual three-phase systems is proposed to separate fundamental current and main harmonics without using LPFs. The diagram is shown in Fig. 5. It consists of two parts, i.e., a standard three-phase PMSM system and a virtual dual three-phase PMSM system. Specifically, through conventional coordinate transformation, the dq-axes currents combined with fundamental and harmonic components are obtained. Meanwhile, the stator current reconstruction using the phase-shifting strategy is carried out, in which the original physical currents are rotated by 30° to obtain additional virtual three-phase currents. The phase-shifting operation is implemented based on a lookup table with respect to the rotor position. Moreover, the physical three-phase currents and virtual three-phase currents constitute the six-phase currents of a dual three-phase machine. Thanks to the harmonic decomposition characteristics of the dual three-phase PMSMs, i_{dqf}, which represents the dq-axes current components without the sixth-order harmonics, can be obtained through VSD transformation. The dq-axes harmonic currents i_{dq6} can be obtained by subtracting i_{dqf} from the output of the standard three-phase system.

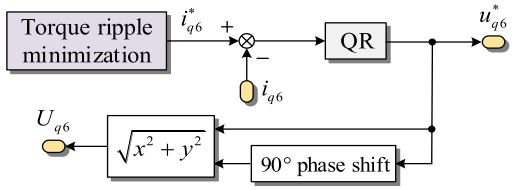

Fig. 6. Diagram of the q-axis harmonic current control.

B. Harmonic Current Regulation Scheme

In the proposed scheme, the harmonics of the d-axis and q-axis are regulated, respectively. Specifically, the q-axis harmonic current is regulated by the control loop, as shown in Fig. 6. According to the torque model-based method [19], the q-axis harmonic current reference was generated by a lookup table of back EMF to reduce the sixth-order torque ripple. It should be noted that the proposed scheme can also be extended to the drive system using the speed feedback to obtain the q-axis harmonic current reference. A quasi-resonant (QR) controller with the resonant frequency set to six times the fundamental frequency is employed to regulate the q-axis harmonic current. The harmonic voltage output by the controller is represented as u^*_{q6}. Then, a simple method based on a phase-shift operator is used to obtain the amplitude U_{q6}, which will be utilized for the calculation of d-axis harmonic voltage based on the geometric principle. Specifically, the output of the QR controller is approximately a sinusoidal signal with a frequency of six times the fundamental frequency. Since $\sin^2\alpha + \cos^2\alpha = 1$, when constructing an auxiliary signal with a phase difference of 90° from the original signal, the amplitude of this sine signal can be calculated using the trigonometric function.

Fig. 7 shows the overall control structure of the proposed harmonic current regulation scheme. First, the fundamental and harmonic currents in the dq-frame are separated by the proposed harmonic detection method. Then, the fundamental currents are controlled as the conventional FOC. The separated q-axis harmonic current is regulated to suppress the torque ripple. Meanwhile, the injected d-axis harmonic voltage for reducing voltage fluctuations is directly calculated by the voltage relationship derived from the geometric principle, which can contribute to minimizing the maximum magnitude of the stator voltage vector. Specifically, (19) and (20) are used to determine the amplitude and phase of the d-axis harmonic voltage, respectively. Noted that voltage regulation here is based on the analytical solution

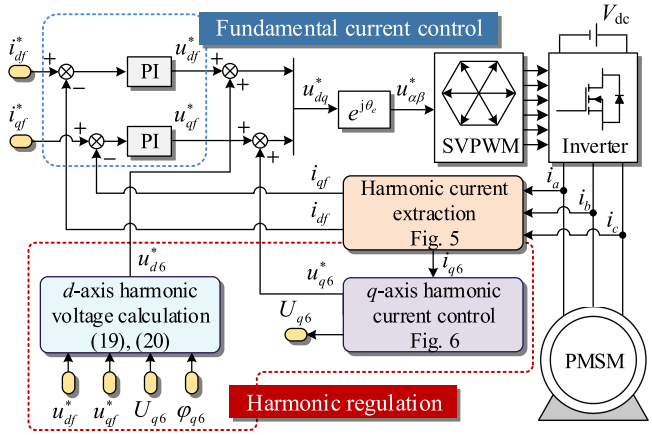

Fig. 7. Diagram of the proposed current control scheme.

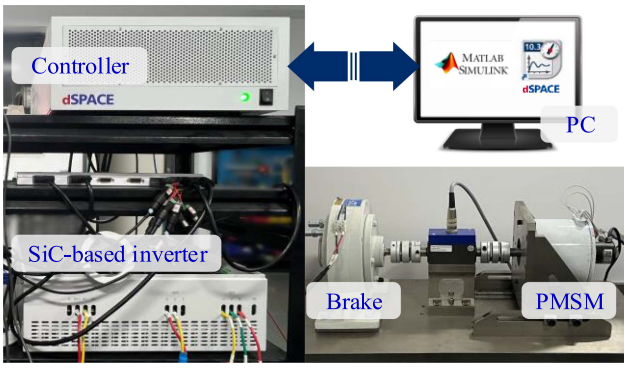

Fig. 8. Schematic diagram of the experimental setup.

TABLE I
PARAMETERS OF THE EXPERIMENTAL PLANT

Parameter	Value
Pole pairs	5
Rated current (A)	4
Rated torque (N·m)	4.8
d-axis inductance L_d (mH)	5.78
q-axis inductance L_q (mH)	5.78
Stator resistance R_s (Ω)	1.89

from the geometric principle, which avoids closed-loop control and can effectively reduce the computational burden. Overall, the proposed control scheme can reduce the torque ripple with high dc-link voltage utilization.

V. EXPERIMENTAL VALIDATION

The proposed scheme is verified experimentally on a setup, as shown in Fig. 8, in which the test SPMSM is loaded by a magnetic brake. Table I presents the main parameters of the test machine whose back-EMF waveforms are shown in Fig. 1. The control scheme is implemented with a dSPACE DS1007 system. The inverter is designed with silicon carbide power modules and powered by a constant voltage source. The sampling and

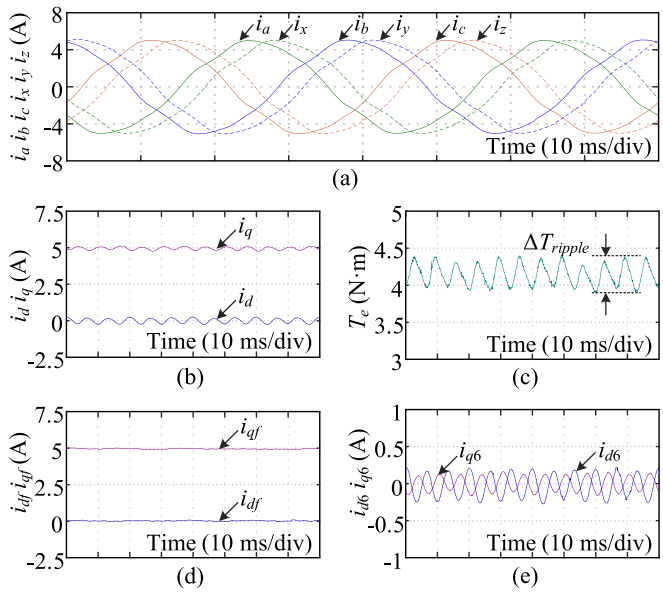

Fig. 9. Experimental results of conventional FOC and the proposed harmonic detection method. (a) Phase currents. (b) dq-axes currents. (c) Output torque. (d) Detected DC components of dq-axes currents. (e) Detected harmonic components of dq-axes currents.

switching frequency is 10 kHz. The experimental drive system operates in speed control mode. All experimental results are captured by the ControlDesk interfaced with the dSPACE system. Since the bandwidth of the torque transducer is limited, the torque waveforms are calculated by the captured phase currents [21], [28]. Specifically, the electromagnetic torque is calculated through $T_e = n_p(e_a i_a + e_b i_b + e_c i_c)/\omega_e$.

Fig. 9 shows the experimental results of conventional FOC and the proposed harmonic detection method. It is noted that, at this time, the harmonic detection method is adopted, but the harmonic control method is not enabled. Obviously, there are harmonics in the stator currents and dq-axes currents caused by nonsinusoidal back EMFs, which lead to torque ripples. Moreover, the obtained virtual currents i_x, i_y, and i_z are also shown in Fig. 9(a). Based on the virtual currents and the proposed harmonic detection method, the fundamental and harmonic components of the dq-axes currents are well separated, as shown in Fig. 9(d) and (e). It should be noted that no LPFs are used in the harmonic detection process, which guarantees the system to operate with decent performance. Furthermore, the detected d-axis and q-axis harmonics will be further regulated to achieve torque ripple suppression and high voltage utilization.

Fig. 10 shows the experimental results of the steady-state performance at 300 r/min with three different methods. The waveforms of three-phase currents, dq-axes currents, electromagnetic torques, and amplitudes of the voltage vector are presented. Two existing methods are selected for comparison with the proposed method, namely Method I and Method II. The sinusoidal current control scheme [17] is referred to as Method I. The optimized q-axis current harmonic injection [19] is referred to as Method II. The waveforms of phase currents, dq-axes currents, output

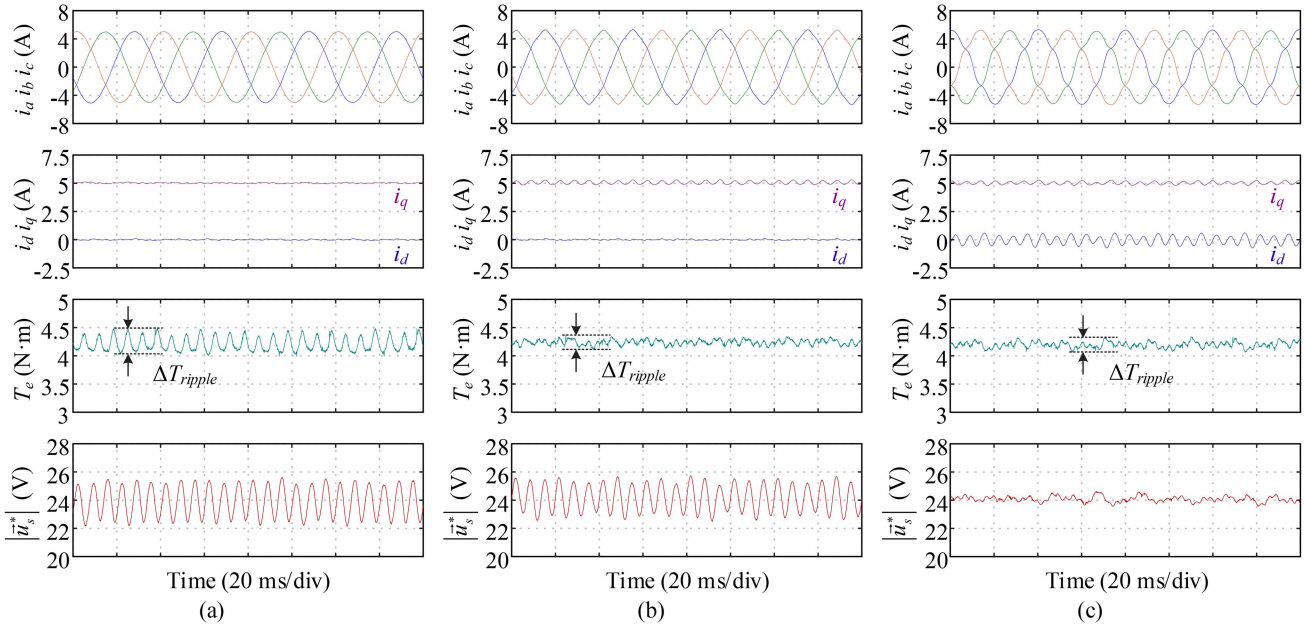

Fig. 10. Experimental results under 300 r/min. (a) Method I. (b) Method II. (c) Proposed method.

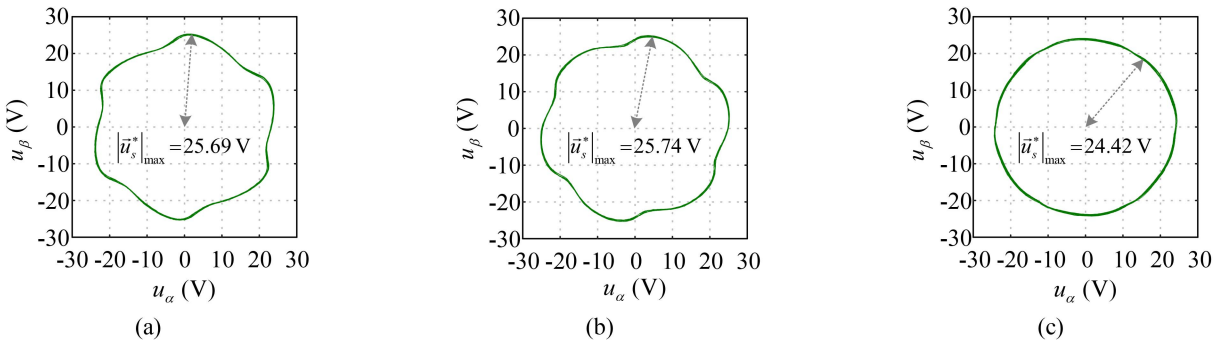

Fig. 11. Comparison of voltage trajectories. (a) Method I. (b) Method II. (c) Proposed method.

torques, amplitudes of the voltage vector, and voltage trajectories are given. As shown in Fig. 10(a), Method I can suppress the harmonic currents to a quite low level. Additionally, the torque ripple is also reduced to a certain extent, but there are still obvious sixth-order fluctuations in the output torque. Then, it can be seen from Fig. 10(b) that the optimal q-axis harmonic currents injected can further reduce the torque ripple. Nevertheless, these two methods will result in fluctuations of voltage amplitude because of the increased harmonic voltages, which is consistent with theoretical analysis. On the contrary, as shown in Fig. 10(c), the proposed method can reduce torque ripple with hardly any voltage fluctuation. It is assumed that the dc-link voltage is limited, and Method I and Method II may not be feasible due to the higher voltage amplitudes required. Comparatively, the proposed method can reduce the torque ripple with high dc-link voltage utilization, which contributes to work well under voltage limits.

To reveal the effectiveness of the proposed method more clearly, Fig. 11 shows the comparison of voltage trajectories, which also indicates that the proposed method can well suppress the sixth-order fluctuations of voltage amplitude. Meanwhile, with the proposed method, the trajectory of the output voltage vector is approximately circular, thereby reducing the maximum value of voltage vector amplitude and improving voltage utilization. The maximum voltage amplitudes for the three methods are 25.69 V, 25.74 V, and 24.42 V, respectively. As discussed in Fig. 2, the minimum dc-link voltage for implementing the above three strategies is 44.50 V, 44.58 V, and 42.30 V, respectively. By applying the proposed method, the dc-link voltage utilization can be improved by approximately 5.4% compared with traditional methods. The results are conducted on a small-scale test rig for verification, and the proposed method can generate more significant benefits in high-power applications, such as offshore wind power generation.

In Fig. 12, fast Fourier transform (FFT) results of phase current under the conventional FOC and three methods for torque ripple reduction are compared. As can be seen, with the sinusoidal current excitation as the control target, the fifth- and seventh-order harmonics of the phase current under Method I are relatively small. On the contrary, when employing Method

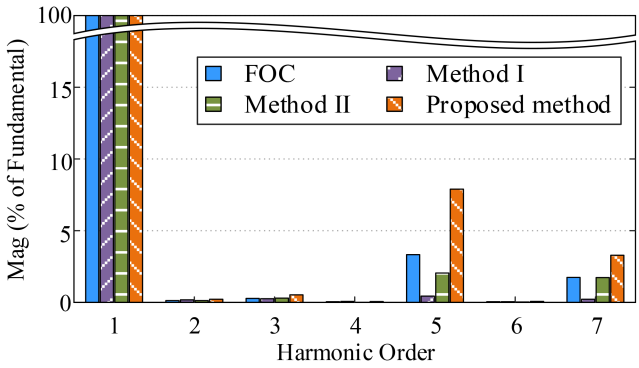

Fig. 12. FFT spectrum of phase current under different methods.

TABLE II
COMPARISON BETWEEN DIFFERENT METHODS

	FOC	Method I	Method II	Proposed method
ΔT_{ripple} (N·m)	0.52	0.45	0.20	0.21
$\lvert\vec{u}_s\rvert_{\max}$ (V)	24.90	25.69	25.74	24.42
P_{Cu} (W)	70.98	70.88	70.93	71.38

II or the proposed method, a few fifth- and seventh-order harmonics are intentionally injected to further enhance the system performance.

To fairly evaluate the cost of harmonic injection, the loss analysis is carried out by which the fundamental and main harmonic currents are considered. The copper loss P_{Cu} is calculated through

$$P_{\mathrm{Cu}} = \frac{3}{2}\left(I_1^2 + I_5^2 + I_7^2\right) R_s \tag{23}$$

where I_1, I_5, and I_7 represent the current amplitudes of the fundamental, fifth, and seventh harmonic currents, respectively. Then, the comparison between all the implemented methods in terms of torque ripple, maximum voltage amplitude, and copper loss is summarized in Table II. As can be seen, compared with the conventional FOC, the proposed method can reduce torque ripple by about 60% and achieve higher voltage utilization. It should be noted that the proposed method results in a slight increase in copper loss because of the higher amplitude of the harmonic current injected. Specifically, the copper loss of the proposed method is only 0.6% higher than that of the conventional FOC, which is acceptable for cases where the temperature margin is relatively large. Furthermore, to reduce torque ripple with the low copper loss, the drive system can use Method II under low-voltage (low-speed) operating conditions and would change to the proposed method when approaching the voltage limits.

Fig. 13 shows the experimental comparison results under different speeds and load conditions. The peak-to-peak values of torque ripple $\Delta T_{\mathrm{ripple}}$ and voltage amplitude ripple $\Delta|\vec{u}_s|_{\mathrm{ripple}}$ with different methods are presented. It can be seen that applying Method I results in a certain torque ripple, which grows larger as the load gets heavier. This is because the PM flux linkage contains certain fifth and seventh harmonics. In contrast, when

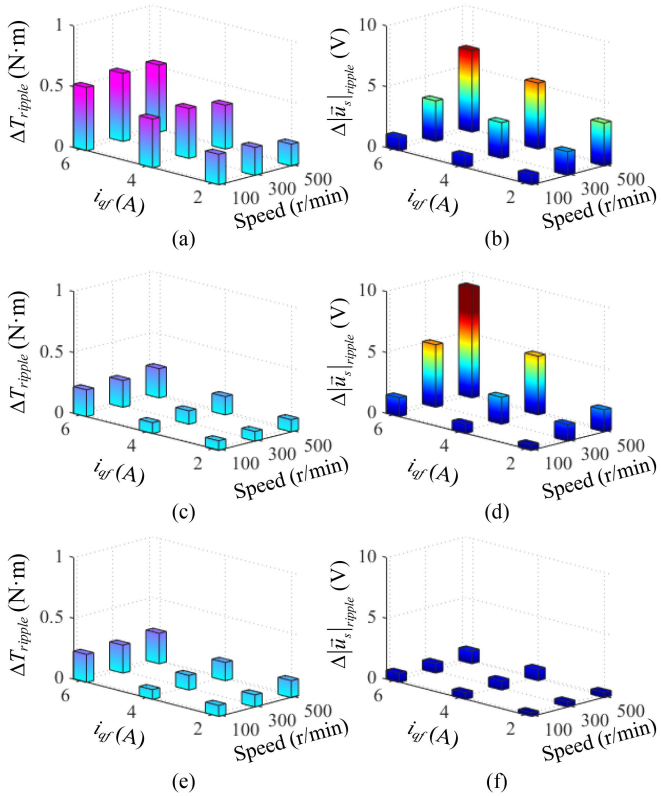

Fig. 13. Experimental results under different speeds and load conditions. (a) Torque ripple with method I. (b) Voltage ripple with method I. (c) Torque ripple with method II. (d) Voltage ripple with method II. (e) Torque ripple with the proposed method. (f) Voltage ripple with the proposed method.

using Method II or the proposed method, the torque ripple under different operating conditions can be suppressed. Moreover, as shown in Fig. 13(b) and (d), both Method I and Method II can result in voltage amplitude ripple. When the speed and load are both relatively high, the voltage fluctuation is very obvious. On the contrary, as can be seen in Fig. 13(f), after using the proposed method, the voltage fluctuation under all conditions can be significantly suppressed.

It should be noted that the used digital filters, such as LPFs, in harmonic regulation of the existing methods can cause significant delay and degrade the transient response. To verify the superiority of the proposed method, the comparison results between the method presented in [25] and the proposed one are given. In [25], several LPFs are used in current harmonic extraction, and one BPF is used for harmonic voltage control. Fig. 14 shows the waveforms of mechanical speed and stator voltage amplitude during the speed accelerating process. The test machine accelerates from 300 to 600 r/min, and the load torque remains unchanged. With increasing mechanical speed, both the stator voltage amplitude and fundamental frequency increase. As shown in Fig. 14(a), when using the method in [25], the stator voltage amplitude exhibits a certain overshoot and transient oscillation. In contrast, as shown in Fig. 14(b), with the proposed scheme, the convergence time of the voltage amplitude control is short and there is almost no significant transient oscillation. This is because the regulation of voltage

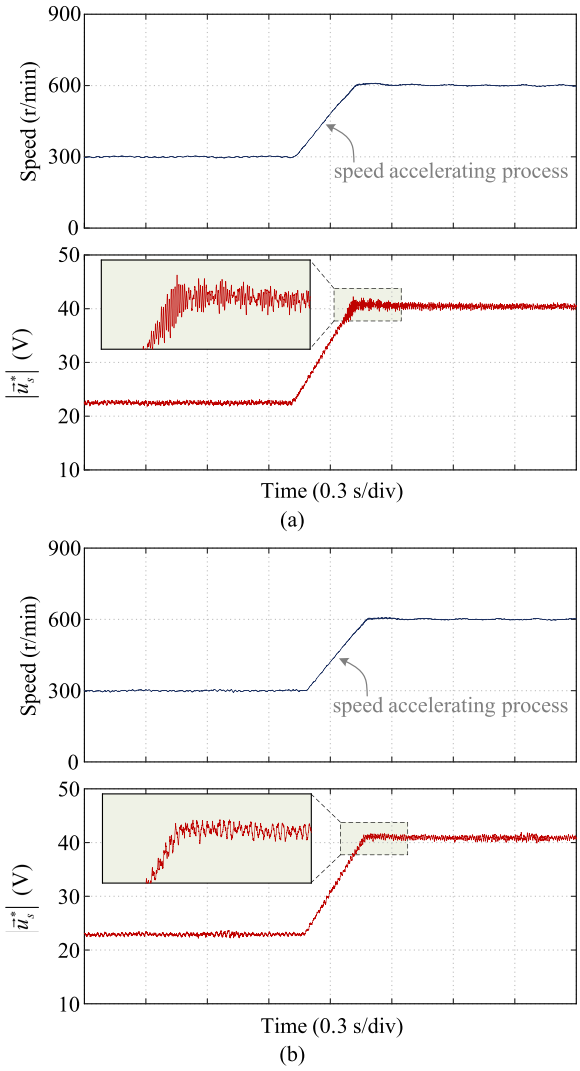

Fig. 14. Experimental results during the speed accelerating process. (a) Method presented in [25]. (b) Proposed method.

amplitude in the proposed scheme is not through closed-loop control but based on the analytical solution from the geometric principle, and no digital filter is used in the overall system.

To sum up, the proposed scheme can achieve decent performance in both steady and transient states.

VI. Conclusion

This article proposes a novel harmonic current regulation for torque ripple reduction of SPMSM drives. It is thoroughly investigated that how harmonic injection affects dc-link voltage utilization. Different from the previous methods, both q-axis and d-axis harmonic currents are systematically optimized and injected. The proposed method has the following advantages.

1) Torque ripple can be suppressed with hardly any voltage fluctuation, which contributes to the high dc-link voltage utilization.
2) The regulation for stator voltage amplitude is based on the analytical solution from the geometric principle, which has relatively low implementation complexity and is independent of machine parameters.
3) No digital filters, such as LPFs, are used in harmonic detection, so there is almost no additional delay introduced in the control loop.

Finally, the effectiveness and advantages of the proposed scheme are verified by the experimental results.

The future work will focus on how the proposed scheme can be extended to interior PMSMs and multiphase machines. Moreover, the magnetic coenergy theory can also be employed to obtain a more accurate torque expression, by which the harmonic current reference can be further optimized, and the torque ripple will be better suppressed accordingly.

References

[1] Z. Q. Zhu and D. Howe, "Electrical machines and drives for electric, hybrid, and fuel cell vehicles," *Proc. IEEE*, vol. 95, no. 4, pp. 746–765, Apr. 2007.
[2] K. T. Chau, C. C. Chan, and C. Liu, "Overview of permanent-magnet brushless drives for electric and hybrid electric vehicles," *IEEE Trans. Ind. Electron.*, vol. 55, no. 6, pp. 2246–2257, Jun. 2008.
[3] V. Yaramasu, B. Wu, P. C. Sen, S. Kouro, and M. Narimani, "High-power wind energy conversion systems: State-of-the-art and emerging technologies," *Proc. IEEE*, vol. 103, no. 5, pp. 740–788, May 2015.
[4] X. Song, H. Wang, X. Ma, X. Yuan, and X. Wu, "Robust model predictive current control for a nine-phase open-end winding PMSM with high computational efficiency," *IEEE Trans. Power Electron.*, vol. 38, no. 11, pp. 13933–13943, Nov. 2023.
[5] X. Zhang, L. Ren, J. Zhao, J.-Y. Gauthier, X. Lin-Shi, and F. Wang, "A boost-type four-leg inverter with integrated open-phase fault-tolerance for PMSM drives," *IEEE Trans. Power Electron.*, vol. 38, no. 12, pp. 15932–15944, Dec. 2023.
[6] N. Nakao and K. Akatsu, "Suppressing pulsating torques: Torque ripple control for synchronous motors," *IEEE Ind. Appl. Mag.*, vol. 20, no. 6, pp. 33–44, Nov./Dec. 2014.
[7] A. H. Abosh, Z. Q. Zhu, and Y. Ren, "Reduction of torque and flux ripples in space vector modulation-based direct torque control of asymmetric permanent magnet synchronous machine," *IEEE Trans. Power Electron.*, vol. 32, no. 4, pp. 2976–2986, Apr. 2017.
[8] J. Huo, N. Zhao, R. Gao, G. Wang, G. Zhang, and D. Xu, "Torque ripple compensation with anti-overvoltage for electrolytic capacitorless PMSM compressor drives," *IEEE J. Emerg. Sel. Topics Power Electron.*, vol. 10, no. 5, pp. 6148–6159, Oct. 2022.
[9] T. M. Jahns and W. L. Soong, "Pulsating torque minimization techniques for permanent magnet AC motor drives—A review," *IEEE Trans. Ind. Electron.*, vol. 43, no. 2, pp. 321–330, Apr. 1996.
[10] N. Bianchi and S. Bolognani, "Design techniques for reducing the cogging torque in surface-mounted PM motors," *IEEE Trans. Ind. Appl.*, vol. 38, no. 5, pp. 1259–1265, Sep./Oct. 2002.
[11] R. Islam, I. Husain, A. Fardoun, and K. McLaughlin, "Permanent-magnet synchronous motor magnet designs with skewing for torque ripple and cogging torque reduction," *IEEE Trans. Ind. Appl.*, vol. 45, no. 1, pp. 152–160, Jan./Feb. 2009.
[12] L. J. Wu, Z. Q. Zhu, D. A. Staton, M. Popescu, and D. Hawkins, "Comparison of analytical models of cogging torque in surface-mounted PM machines," *IEEE Trans. Ind. Electron.*, vol. 59, no. 6, pp. 2414–2425, Jun. 2012.
[13] K. Wang, Z. Q. Zhu, and G. Ombach, "Torque enhancement of surface-mounted permanent magnet machine using third-order harmonic," *IEEE Trans. Magn.*, vol. 50, no. 3, Mar. 2014, Art. no. 8100210.
[14] Y. Liu, Z. Q. Zhu, and D. Howe, "Direct torque control of PM brushless AC motors having non-sinusoidal back-emf waveforms," in *Proc. 3rd IET Int. Conf. Power Electron., Mach. Drives*, 2006, pp. 425–429.
[15] S.-H. Hwang and J.-M. Kim, "Dead time compensation method for voltage-fed PWM inverter," *IEEE Trans. Energy Convers.*, vol. 25, no. 1, pp. 1–10, Mar. 2010.
[16] C. Shang, M. Yang, J. Long, D. Xu, Jun Zhang, and J. Zhang, "An accurate VSI nonlinearity modeling and compensation method accounting for DC-link voltage variation based on LUT," *IEEE Trans. Ind. Electron.*, vol. 69, no. 9, pp. 8645–8655, Sep. 2022.

[17] H. Kim, Y. Han, K. Lee, and S. Bhattacharya, "A sinusoidal current control strategy based on harmonic voltage injection for harmonic loss reduction of PMSMs with non-sinusoidal back-EMF," *IEEE Trans. Ind. Appl.*, vol. 56, no. 6, pp. 7032–7043, Nov./Dec. 2020.
[18] G. Liu, B. Chen, K. Wang, and X. Song, "Selective current harmonic suppression for high-speed PMSM based on high-precision harmonic detection method," *IEEE Trans. Ind. Inform.*, vol. 15, no. 6, pp. 3457–3468, Jun. 2019.
[19] P. Mattavelli, L. Tubiana, and M. Zigliotto, "Torque-ripple reduction in PM synchronous motor drives using repetitive current control," *IEEE Trans. Power Electron.*, vol. 20, no. 6, pp. 1423–1431, Nov. 2005.
[20] H. Jia, M. Cheng, W. Hua, W. Zhao, and W. Li, "Torque ripple suppression in flux-switching PM motor by harmonic current injection based on voltage space-vector modulation," *IEEE Trans. Magn.*, vol. 46, no. 6, pp. 1527–1530, Jun. 2010.
[21] J. Qu, J. Jatskevich, C. Zhang, and S. Zhang, "Torque ripple reduction method for permanent magnet synchronous machine drives with novel harmonic current control," *IEEE Trans. Energy Convers.*, vol. 36, no. 3, pp. 2502–2513, Sep. 2021.
[22] C. Xia, B. Ji, and Y. Yan, "Smooth speed control for low-speed high-torque permanent-magnet synchronous motor using proportional–integral–resonant controller," *IEEE Trans. Ind. Electron.*, vol. 62, no. 4, pp. 2123–2134, Apr. 2015.
[23] G. Feng, C. Lai, J. Tian, and N. C. Kar, "Multiple reference frame based torque ripple minimization for PMSM drive under both steady-state and transient conditions," *IEEE Trans. Power Electron.*, vol. 34, no. 7, pp. 6685–6696, Jul. 2019.
[24] L. Yan, Y. Liao, H. Lin, and J. Sun, "Torque ripple suppression of permanent magnet synchronous machines by minimal harmonic current injection," *IET Power Electron.*, vol. 12, no. 6, pp. 1368–1375, 2019.
[25] L. Wu and Z. Lyu, "Harmonic injection-based torque ripple reduction of PMSM with improved DC-link voltage utilization," *IEEE Trans. Power Electron.*, vol. 38, no. 7, pp. 7976–7981, Jul. 2023.
[26] Y. Zhao and T. A. Lipo, "Space vector PWM control of dual three-phase induction machine using vector space decomposition," *IEEE Trans. Ind. Appl.*, vol. 31, no. 5, pp. 1100–1109, Sep./Oct. 1995.
[27] L. Yan et al., "Multiple synchronous reference frame current harmonic regulation of dual three phase PMSM with enhanced dynamic performance and system stability," *IEEE Trans. Ind. Electron.*, vol. 69, no. 9, pp. 8825–8838, Sep. 2022.
[28] L. Wu, Y. Guo, X. Huang, Y. Fang, and J. Liu, "Harmonic torque suppression methods for single-phase open-circuit fault-tolerant operation of PMSM considering third harmonic BEMF," *IEEE Trans. Power Electron.*, vol. 36, no. 1, pp. 1116–1129, Jan. 2021.

Zekai Lyu (Graduate Student Member, IEEE) received the B.Eng. degree from Southwest Jiaotong University, Chengdu, China, in 2018, and the M.Sc. degree from the Harbin Institute of Technology, Harbin, China, in 2020, both in electrical engineering. He is currently working toward the Ph.D. degree in electrical engineering with Zhejiang University, Hangzhou, China.

His current research interests include wide-bandgap device applications and electrical machine drives.

Mr. Lyu was a recipient of the Best Presenter Award at the 2022 IEEE Transportation Electrification Conference and Expo, Asia-Pacific (ITEC Asia-Pacific 2022).

Lijian Wu (Senior Member, IEEE) received the B.Eng. and M.Sc. degrees from the Hefei University of Technology, Hefei, China, in 2001 and 2004, respectively, and the Ph.D. degree from the University of Sheffield, Sheffield, U.K., in 2011, all in electrical engineering.

From 2004 to 2007, he was an Engineer with Delta Electronics (Shanghai) Company, Ltd. From 2012 to 2013, he was with Sheffield Siemens Wind Power Research Center as a Design Engineer focusing on wind power generators. From 2013 to 2016, he was an advanced Engineer with Siemens Wind Power A/S, Brande, Denmark. Since 2016, he has been with Zhejiang University, Hangzhou, China, where he is currently a Professor of electrical machines and control systems. His current major research interests include the design and control of permanent magnet machines.

Pingyue Song received the B.Eng. degree in electrical engineering from the Hebei University of Technology, Tianjin, China, in 2021. He is currently working toward the Ph.D. degree in electrical engineering with Zhejiang University, Hangzhou, China.

His current research interests include control of motor-drive systems and sensor error compensation.